Chemistry Europe
European Chemical Societies Publishing

Structure of Diethyl-Phosphonic Acid Anchoring Group Affects the Charge-Separated State on an Iridium(III) Complex Functionalized NiO Surface

Ruri Agung Wahyuono[+],[a, b] Sebastian Amthor[+],[c] Carolin Müller,[a, b] Sven Rau,*[c] and Benjamin Dietzek*[a, b, d]

Cyclometalated Iridium(III) complexes, *i.e.* $[Ir(CN)_2(dppz)][PF_6]$, bearing either two or four $-CH_2PO(OH)_2$ anchoring groups (**IrP_2dppz** or **IrP_4dppz**) are explored as photosensitizers for p-type dye sensitized solar cell (DSSC). The synthetic route is described and the iridium(III) complexes are characterized with respect to their electrochemical and photophysical properties. The modified anchoring ligand geometry exploited in this work not only alters the electronic nature of the complex (that is by destabilizing the LUMO energetically) but more importantly improves the grafting ability of the complex towards the NiO surface. The photoinduced long-lived charge separated state (CSS) at the **NiO**|**IrP_xdppz** interface is of a different nature comparing the two complexes. For **IrP_2dppz** and **IrP_4dppz** the electron density of the CSS dominantly resides on the dppz and the CN ligand, respectively. The stability of the CSS can be correlated to the solar cell performance in NiO-based p-DSSCs, which yield conversion efficiencies which are among the highest in the class of iridium(III) complexes developed for p-DSSCs.

1. Introduction

The development and improvement of dye-sensitized photocathodes might enable tandem dye-sensitized solar cells (DSSCs) as well as photocathodes for H_2 generation or CO_2 reduction.[1,2] Despite significant improvements the performance of p-DSSCs ($\eta = 2.51\%$) remains inferior compared to their counterpart n-DSSCs ($\eta > 13\%$).[3] The low efficiency (η) of p-DSSCs roots in the rapid recombination of the charge-separated states typically within a few hundred ps. Thus, rapid hole injection from the dye into the valence band (VB) of NiO and the lifetime of the charge-separated state (CSS), $h^+(NiO)|Dye^{\bullet-}$, are the key to be optimized.[4] Molecular design for sensitizers in p-DSSCs requires the highest occupied molecular orbital (HOMO) to be localized in the proximity to the NiO surface, ideally with orbital overlap to the VB orbitals of NiO. Meanwhile, the lowest unoccupied molecular orbital (LUMO) extends away from the NiO surface.[1–5]

To date the organic push-pull dyes serve as benchmark photosensitizers for NiO-based p-DSSCs.[6–8] However, also Ruthenium complexes, more specifically structural derivatives of the paradigm photosensitizer $[Ru(bpy)_3]^{2+}$ (bpy = 2,2′-bipyridine), perform comparably well.[9–15] To increase the performance of Ru(II)-complex sensitized photocathodes, modifications of the ancillary, *i.e.* the non-anchoring ligand have been introduced. Such modifications include, *e.g.*, trifluoromethyl-substitution[10] and a π-extension of the ligand utilizing dipyridophenazine (dppz) ancillary ligands.[11] Both approaches stabilize the charge separated states by pushing the electron density away from the NiO surface.[10,11] Recently, cyclometalated Ruthenium(II) complexes $[Ru(NN)_2(CN)]^+$ complexes [NN = diimine ligand, CN = bidentate cyclometalated phenylpyridine (ppy)] have been suggested as promising lead structures for molecular photosensitizers in p-DSSCs.[12–15] The HOMO, localized on the Ruthenium ion, extends to the anionic phenyl ring of ppy ligand whilst the LUMO is localized on the NN ligand.[16,17] Thus, various anchoring groups such as carboxylic acid, phosphonic acid, or catechol, can be introduced to the cyclometalated ligand.[18] This design concept can be extended to cyclometalated Iridium(III) complexes. Their excited-state are strong oxidants thus favoring hole injection to the VB of NiO.[19–25] Recently, Odobel and co-workers systematically studied the performance of Iridium(III) photosensitizers with different anchoring groups in the presence of various

[a] R. A. Wahyuono,[+] C. Müller, Prof. Dr. B. Dietzek
Department Functional Interfaces
Leibniz Institute of Photonic Technology (IPHT) Jena e.V.
Albert-Einstein-Straße 9, 07745 Jena (Germany)
E-mail: benjamin.dietzek@leibniz-ipht.de
[b] R. A. Wahyuono,[+] C. Müller, Prof. Dr. B. Dietzek
Institute of Physical Chemistry
Friedrich Schiller University Jena
Helmholtzweg 4, 07743 Jena (Germany)
[c] S. Amthor,[+] Prof. Dr. S. Rau
Institute of Inorganic Chemistry I
University Ulm
Albert-Einstein-Allee 11, 89081 Ulm (Germany)
E-mail: sven.rau@uni-ulm.de
[d] Prof. Dr. B. Dietzek
Center for Energy and Environmental Chemistry (CEEC)
Friedrich Schiller University Jena
Philosophenweg 7a, 07743 Jena (Germany)
[+] These authors contributed equally to this work.

Supporting information for this article is available on the WWW under https://doi.org/10.1002/cptc.202000038

redox mediators:[21] Long-lived CSS, which are key to DSSC performance, were achieved by using anchoring groups electronically decoupled from the dye.[18,21]

In this study, cyclometalated Iridium(III) complexes with a π-accepting dipyridophenazine (dppz) ancillary ligand are exploited for p-DSSCs. The complexes are functionalized with phosphonic acid anchoring groups electronically decoupled from the chromophore by a CH_2-group (see Figure 1). A phosphonic acid anchor joined via a CH_2 spacer yields a more stable linkage towards the metal oxide surface than carboxylic acids in aqueous media[26] while at same time providing a sufficiently strong electronic coupling between C^N ligand and NiO, which results in a rapid hole injection.[27] In addition, the effect of two or four anchoring groups, *i.e.* **IrP$_2$dppz** and **IrP$_4$dppz** (Figure 1) to the photoinduced charge separation in the photocathode and the resultant p-DSSCs will be investigated.

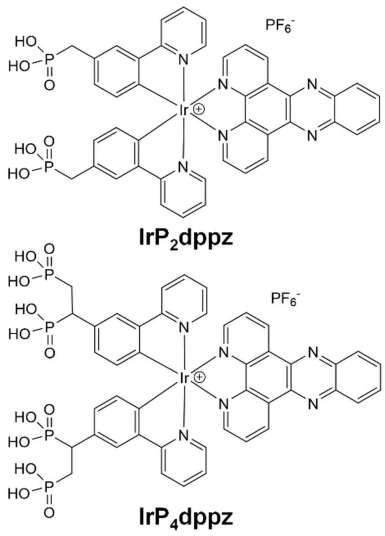

Figure 1. Structure of cyclometalated iridium(III) complexes bearing either two (**IrP$_2$dppz**) or four phosphonic acid (**IrP$_4$dppz**) anchoring groups.

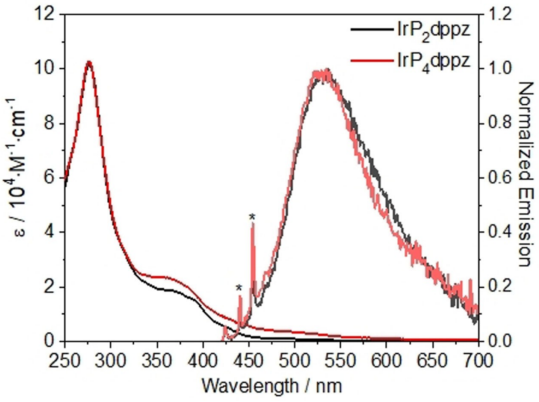

Figure 2. UV/Vis absorption and emission spectra of **IrP$_2$dppz** and **IrP$_4$dppz** in solution. The emission spectra were recorded upon excitation at 355 nm. Peaks at emission spectra marked with asterisk [*] are the Raman scattering from the solvent mixture, *i.e.* H_2O:ACN (1:9, %v/v).

2. Results and Discussion

2.1. Optical and Electrochemical Properties

The UV/Vis absorption and emission spectra of **IrP$_2$dppz** and **IrP$_4$dppz** in a mixture of H_2O:ACN (1:9, %v/v) are shown in Figure 2 and the photophysical data is summarized in Table 1. The specific solvent mixture containing H_2O was used for solubility reasons as the compounds exhibit very low solubility in purely organic solvents, due to their high amount of phosphonic acid moieties. The absorption spectra of both complexes feature an intense absorption at 275 nm due to spin-allowed π-π* ligand-centered (^{1}LC) transition on the dppz ligand.[23] The absorption bands between 350 to 400 nm are attributed to ^{1}MLCT (metal-to-ligand charge transfer) and ^{1}LLCT (ligand-to-ligand charge transfer) transitions. The visible absorption band stems from triplet states due to the strong spin-orbit coupling.[19–25] Despite the weak absorption in the visible regime, the extinction coefficient of **IrP$_4$dppz** (0.6×10^4 $M^{-1}\cdot cm^{-1}$ at 450 nm) is higher than that of **IrP$_2$dppz** (0.2×10^4 $M^{-1}\cdot cm^{-1}$). Quantum chemical studies on related Ir-dppz complexes bearing carboxylic acid anchoring groups reveal that the LUMO is localized on the pyrazine part of the dppz ligand, while the HOMO is localized on both the Iridium metal center and the anchoring cyclometalated C^N ligands.[23]

The MLCT absorption band of **IrP$_2$dppz** at 383 nm is slightly blue-shifted upon introducing two additional anchoring groups in **IrP$_4$dppz**. In line with the absorption shift, a slight hypsochromic shift (40 meV) is found for **IrP$_4$dppz** compared to the emission maximum of **IrP$_2$dppz** at 533 nm. This indicates that the electronic nature of **IrP$_2$dppz** is altered by the addition of the two additional anchoring groups. Both complexes show

Table 1. Photophysical and electrochemical properties of **IrP$_2$dppz** and **IrP$_4$dppz**.

Dye	λ_{abs} [ε][a]	λ_{em} [τ][b]	E_{ox}[c]	$E_{red,1}$[c]	$E_{red,2}$[c]	$E_{red,3}$[c]	$E_{red,4}$[c]	E_{0-0}[d]	ΔG_{inj}[e]	ΔG_{reg}[f]
IrP$_2$dppz	276 (10.2), 362 (1.9), 383 (1.7)	533 (23.9)	+0.82	−1.32	−1.66	−1.83	−2.10	2.64	−1.43	−1.06
IrP$_4$dppz	274 (10.1), 358 (2.4), 376 (2.1), 478* (0.2)	523 (14.4)	+0.82	−1.39	−1.62	−2.06	−2.35	2.62	−1.35	−1.12

[a] λ_{abs} in nm. ε in $10^4\times M^{-1}\cdot cm^{-1}$. Asterisk indicates an absorption shoulder. The extinction coefficient of IrP$_2$dppz was determined in an H_2O:ACN mixture (5:95, %v/v) while for IrP$_4$dppz the corresponding ethyl ester (IrP$_4$dppz^{Et}) was used due to solubility reasons. [b] Given in ns. Emission lifetime was measured using time-correlated single photon counting. [c] In V vs $Fc^{+/0}$. Cyclic voltammograms were collected at an iridium(III) complex concentration of 2 mM in a 0.1 M solution of n-Bu_4NPF_6 in ACN and at a scan rate of 100 mV s^{-1} at 25 °C. [d] E_{0-0} (in eV) is approximated from the crossing point of normalized absorption and emission spectra.[29a] [e] ΔG_{inj} is estimated according to: $\Delta G_{inj} = E_{VB}(NiO) - E_{red}(D^*/D^-)$, where $E_{VB}(NiO)$ is −0.12 V vs. $Fc^{+/0}$ and $E_{red}(D^*/D^-) = E_{red}(D/D^-) + E_{0-0}$. [f] ΔG_{reg} is estimated according to: $\Delta G_{reg} = E_{red}(D/D^-) - E(I_3^-/I^-)$, where $E(I_3^-/I^-)$ is 0.11 V vs. SCE[29b] which was referenced to $Fc^{+/0}$ by subtracting 0.38 V.[29c]

weak ^{3}MLCT phosphorescence in acetonitrile water mixtures[20,25] with an emission quantum yield of about 0.002.

Cyclic voltammetry of **IrP$_2$dppz** and **IrP$_4$dppz** revealed a quasi reversible one-electron oxidation at +0.82 V (*vs.* Fc$^+$/Fc). Both complexes exhibit four reversible reductions, which occur for **IrP$_2$dppz** at −1.33, −1.66, −1.83, and −2.10 V *vs.* Fc$^+$/Fc. At −1.33 V the pyrazine part of the dppz ligand is reduced,[11] while the other three reduction potentials are due to the reduction of the phenanthroline part of the dppz ligand and the CN ligands. The additional phosphonic anchoring groups in **IrP$_4$dppz** cause cathodic shifts of the CN ligand reductions by about 250 mV. Based on the oxidation and third reduction potentials the HOMO-LUMO^{CN} gap for **IrP$_2$dppz** and **IrP$_4$dppz** has been estimated to 2.65 and 2.88 eV, respectively. Meanwhile, the HOMO-LUMO^{dppz} gap is estimated to be 2.11 (**IrP$_2$dppz**) and 2.20 eV (**IrP$_4$dppz**). A higher HOMO-LUMO gap in **IrP$_4$dppz** is in line with the blue shift observed in MLCT absorption band as compared to **IrP$_2$dppz**. The LUMO level localized on both CN and dppz ligand is destabilized in **IrP$_4$dppz** (Figure 3). This LUMO destabilization likely causes the LUMO^{dppz} of **IrP$_4$dppz** to be at approximately the same energy as the LUMO^{CN} of **IrP$_2$dppz**. The different LUMO^{dppz} energies in both complexes can tentatively be correlated to different degrees of bonding interaction between the Iridium centers and the cyclometalated ligands with the pyrazine moiety of dppz, a phenomenon recently observed for Pt-dihalogenido complexes bound to tpphz ligands.[28] The joint electrochemical and photophysical data can be used to estimate the Gibbs free energies for hole injection (ΔG_{inj}) and dye regeneration (ΔG_{reg}), when the complexes are used to sensitize NiO (Table 1): Both hole injection and dye regeneration are thermodynamically favorable for both **IrP$_2$dppz** and **IrP$_4$dppz**. ΔG_{inj} is significantly more negative compared to Ru^{II} complexes on NiO, for which literature reports typical values for ΔG_{inj} in the range from −0.2 to −0.5 eV.[11–15] These numbers imply a very efficient hole injection that will be investigated using time resolved spectroscopy (*vide infra*).

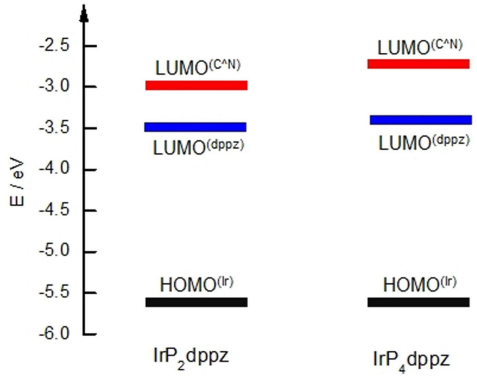

Figure 3. Molecular orbital energy of IrP2dppz and IrP4dppz estimated from the electrochemical data: HOMO = −(Eox + 4.8) eV and LUMO = −(Ered + 4.8) eV.

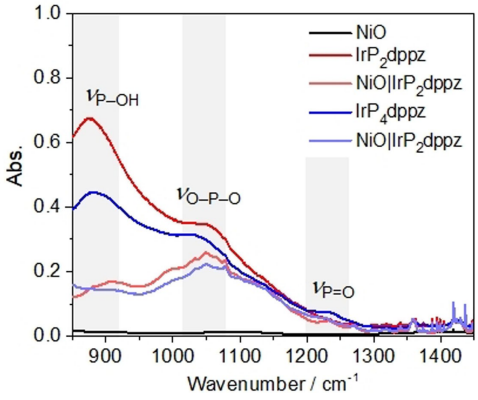

Figure 4. ATR-IR spectra of **IrP$_2$dppz** and **IrP$_4$dppz** measured both in solution and grafted on NiO.

The grafting of **IrP$_2$dppz** and **IrP$_4$dppz** onto NiO was assessed by ATR IR spectroscopy (Figure 4). Typically, IR active vibrations at 1210 cm^{-1} (P=O stretch), 1168 cm^{-1} (P–C stretch), 1000–1100 (O–P–O stretches), and 900–1000 cm^{-1} (P–OH stretches) characterize a phosphonic acid anchoring group.[30] Upon grafting of the complexes to NiO, the intensity of the IR band at 900 cm^{-1} decreases significantly indicating the complexes are bound to NiO surface *via* P–OH. Considering the loss of IR intensity at 900 cm^{-1} upon grafting on NiO, it is likely that all phosponic acid in **IrP$_2$dppz** are anchored to the surface, while two or three phosponic acid groups in **IrP$_4$dppz** are bound to the surface. This result indicates that **IrP$_4$dppz** might yield stronger and more stable adsorption on NiO surface than **IrP$_2$dppz**. Furthermore, the frequency difference ($\Delta\nu = \nu_{as} - \nu_s$)[26a] between asymmetric and symmetric vibration of PO or P–OH in solution ($\Delta\nu_{free}$) and grafted on NiO ($\Delta\nu_{ads}$) yields insight into the binding mode. Since $\Delta\nu_{ads} < \Delta\nu_{free}$ for **IrP$_2$dppz** and **IrP$_4$dppz**, the phosphonic anchoring groups likely binds in a bidentate manner, *i.e.* yielding a stable sensitization as prerequisite for photoinduced charge transfer between the photoexcited sensitizers and the NiO.

The emission lifetimes of **IrP$_2$dppz** and **IrP$_4$dppz** in solution (H_2O:ACN mixture, 1:9, %v/v) (23.9 and 14.3 ns, respectively, Figure 5) are relatively short compared to typical Iridium(III) complexes with emission lifetimes from hundreds ns to µs.[21–23] This short emission lifetime is attributed to emission quenching due to hydrogen bonding of the solvent to the pyrazine-N atoms of the dppz ligand.[31] Grafting of the complexes onto the redox-inert ZrO_2 surface yields a fast decay within the experimental response and an additional slow component, which is characterized by a lifetime of $\tau = 7.3$ and 11.2 ns for **IrP$_2$dppz** and **IrP$_4$dppz**, respectively. While the fast component is attributed to the experimental response function the ns-decay time recorded for the complexes on ZrO_2 is comparably shorter than the lifetime measured in solution. This shortened emission lifetime upon grafting the complexes onto ZrO_2 likely originates from self-quenching due to high density of complexes immobilized on ZrO_2.[32] Upon grafting the complexes to a NiO surface the lifetime is further significantly shortened to $\tau = 2.0$ and 3.4 ns for **IrP$_2$dppz** and **IrP$_4$dppz**, respectively. As previously described in literature,[9,11] the quenching of the sensitizers emission on NiO indicates hole injection from the photoexcited Iridium(III) complex to NiO.

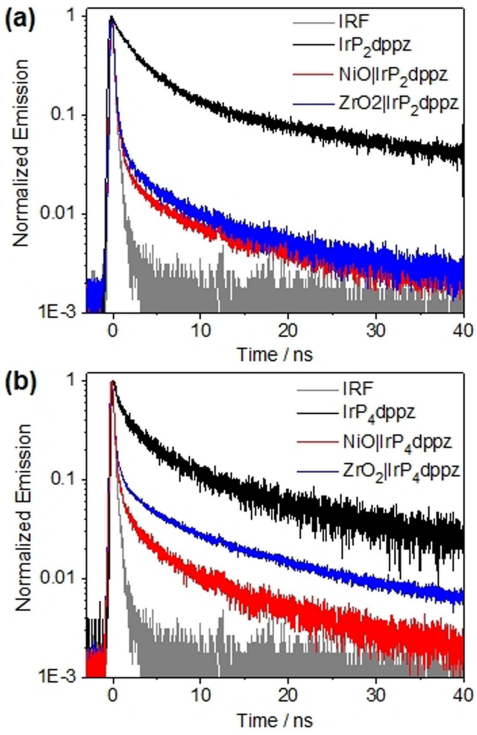

Figure 5. Time-resolved emission decay of (a) **IrP_2dppz** and (b) **IrP_4dppz** in solution (H_2O:ACN mixture, 1:9, %v/v), on a redox inert surface ZrO_2, and on a NiO surface measured using time-correlated single photon counting. The excitation wavelength was centered at 398 nm. Emission of immobilized dye was measured by time-correlated single photon counting (TCSPC) in ambient air.

2.2. Femtosecond Transient Absorption Spectroscopy

Both **IrP_2dppz** and **IrP_4dppz** were studied in solution by ultrafast transient absorption upon excitation at 400 nm, where both MLCT and LLCT transitions are excited.[23] The transient absorption data (Figure 6) exhibit two distinct peaks at 460 and 580 nm, which are assigned to excited state absorption of cyclometalating CN ligand ($^3MLCT^{CN}$) and dppz ligand ($^3MLCT^{dppz}$), respectively. This assignment is based on UV/vis-spectroelectrochemical (SEC) data (Figure S25 and Figure S26 in the Supporting Information) and literature,[25,31] which shows characteristic absorption peaks at 450 and 550 nm upon reduction of the CN and the dppz ligand, respectively (see also grey spectra in Figure 6e and Figure 6f). At early delay time, *e.g.* 0.5 ps, the intensity ratio of the ESA bands at 460 to 560 nm is 1.71 and 0.95 for **IrP_2dppz** and **IrP_4dppz**, respectively. This points to the fact that photoexcitation of **IrP_2dppz** at 400 nm more preferentially excites an MLCT transition towards the CN ligand as compared to the excitation in **IrP_4dppz**. This is in line with the destabilization of the $LUMO^{CN}$ as already inferred from the electrochemical data (*vide supra*).

A quantitative analysis of the transient absorption data is based on a global fit of a sum of exponential functions including an infinite component representing the long-lived signal contribution, which does not decay within the range of experimentally accessible delay times. The result of the fit, in terms of kinetic traces and decay-associated spectra (DAS) is depicted in Figure 6. The time characteristic first-order constants obtained from the fit are summarized in Table 2. The first kinetic components associated with $\tau_1 = 0.3$ ps (**IrP_2dppz**) and 1.3 ps (**IrP_4dppz**) reflect slight blue shifts of the ESA features at 460 and 570 nm. Hence, τ_1 is assigned to vibrational cooling of the $^3MLCT^{CN}$ and $^3MLCT^{dppz}$. Inter system crossing (ISC) form the initially populated singlet state to the triplet manifold is known to occur on ultrafast timescales, *i.e.* <100 fs.[33a] Hence, ISC escapes from the detection with the experimental setup used in this study. The kinetic components associated with $\tau_2 = 17$ ps (**IrP_2dppz**) and 22 ps (**IrP_4dppz**) exhibit a decay of ESA at 450 nm and buildup of signal at 560 nm. Following the assignment of DAS spectra of similar molecules in Ru(II) complexes bearing dppz ligand,[33a,b] these kinetics are assigned to decay of the equilibrated $^3MLCT^{dppz}$ state into an intra-ligand charge transfer (ILCT) state localized on the phenazine part of dppz ligand. Following the photophysics of the transition metal complexes carrying the dppz ligand[33a,b] the kinetic process associated with τ_2 reflects an electron density shift from the phenanthroline (phen) moiety coordinating the Ir(III) ion to the central phenazine (phz) moiety of the ligand, *i.e.* $^3MLCT^{dppz\rightarrow phen} \xrightarrow{\tau_2} {}^3MLCT^{dppz-phz}$. This process is generally manifested in a dispersion shaped decay-associated spectrum as observed here for DAS(τ_2). In correlation to the UV/vis-SEC spectra shown as shaded area spectra in Figure 6(e, f) one should point out that the first reduction of the dppz ligand reduces the phz moiety instead of the phen part of the ligand.[11,33] Hence, the spectral features observed in the UV/vis-SEC mimic the absorption of the $^3MLCT^{dppz-phz}$ state, whose formation is reflected in DAS(τ_2). DAS(τ_3) and DAS(τ_4), which are spectrally similar for both complexes, reflect the decay of the ESA bands at 460 and 570 nm. τ_3 (731 ps (**IrP_2dppz**) and 303 ps (**IrP_4dppz**)) reflects a stronger contribution of signal decay at 570 nm compared to the long-lived component. Based on the spectroelectrochemical analysis (*vide supra*) τ_3 thus reflects partial decay of the $^3MLCT^{dppz-phz}$ state, which is typically observed in Ru-dppz complexes on a sub-ns timescale in water containing solvents.[34] This rapid decay of the $^3MLCT^{dppz-phz}$ is due to interactions of the water molecules and the phz part of the dppz-ligand due to intermolecular hydrogen bonds.[31] The >2-ns component (τ_4) indicates the decay of the resultant long-lived excited state, likely a mixed $^3MLCT^{CN}/^3MLCT^{dppz}$ state to the ground state.

Upon immobilization on NiO surface the transient absorption spectra of both complexes are markedly changed (Figure 7). For **NiO | IrP_2dppz**, the transient absorption data at early

Table 2. Characteristic time constants determined from the global fit of transient absorption data of **IrP_2dppz** and **IrP_4dppz** recorded in solution and on NiO.

System	τ_1 [ps]	τ_2 [ps]	τ_3 [ns]	τ_4 [ns]
IrP_2dppz	0.3	17	0.7	>2
NiO | IrP_2dppz	4.2	189	>2	–
IrP_4dppz	1.3	22	0.3	>2
NiO | IrP_4dppz	8.2	400	>2	–

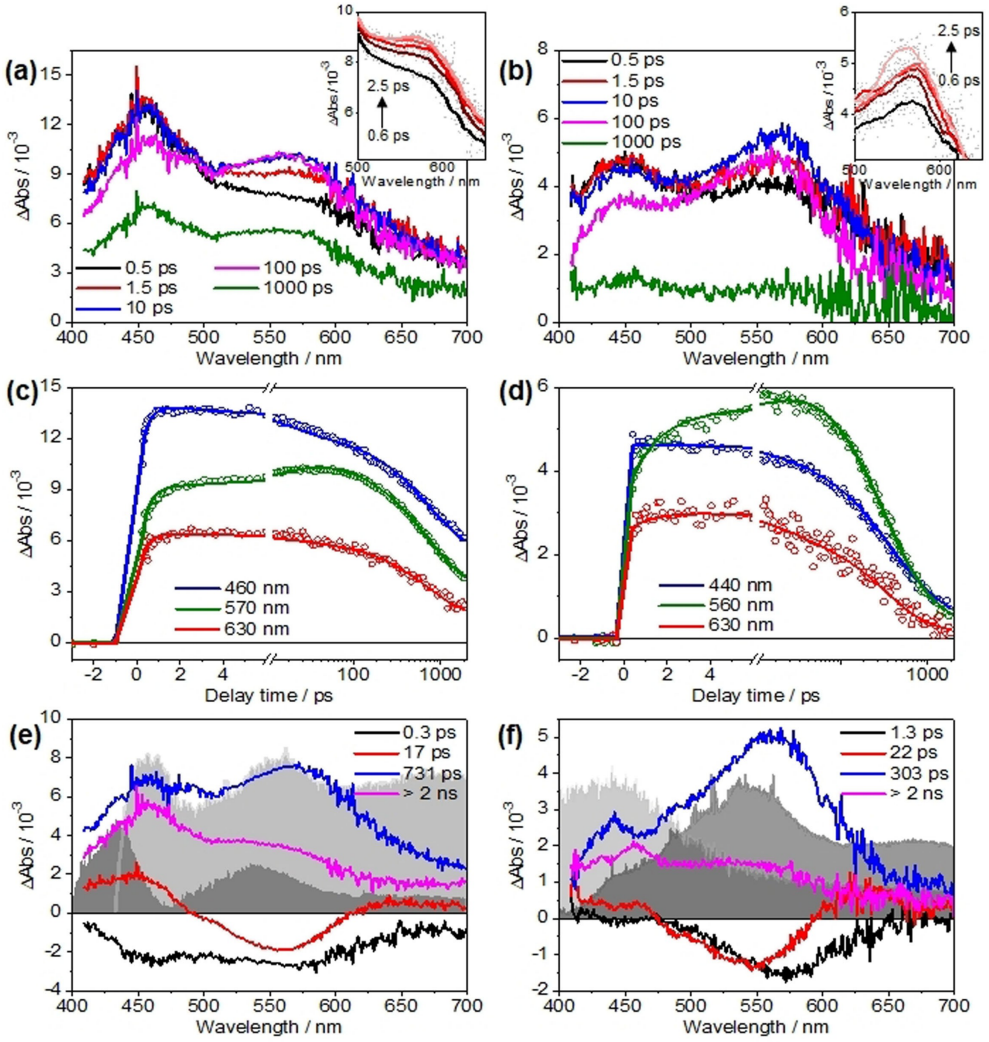

Figure 6. Transient absorption spectra at different delay times, kinetic traces at selected wavelengths, and the decay-associated spectra of **IrP$_2$dppz** (a,c,e) and **IrP$_4$dppz** (b,d,f) measured in solution containing water:ACN mixture (1 : 9, %v/v). Inset of (a) and (b) depicts transient absorption spectra at early delay times. The excitation wavelength was 400 nm with an optical power of 0.21 mW. The grey area in panel (e,f) depict the absorption-difference spectra upon electrochemical reduction of dppz (dark grey) and the CN (light grey) ligand. The absorption-difference spectra (Figure S25 and Figure S26 in the Supporting Information for **IrP$_2$dppz** and **IrP$_4$dppz**, respectively) are arbitrarily scaled to the figure.

time delay show a positive ΔAbs peaking at 580 nm while the signal at 460 nm becomes only barely visible. In contrast, the transient absorption data for **NiO**|**IrP$_4$dppz** display a band at 460 nm, which is slightly stronger than the signal at 560 nm. The results qualitatively indicate that the electronic properties of the two complexes are altered upon immobilization on NiO.

A global fit using a bi-exponential function (including an infinite component) was sufficient to account for the transient absorption data observed for the Iridium(III) complex|NiO interface. The corresponding DAS are depicted in Figure 7 and the corresponding time constant are listed in Table 2. For both **NiO**|**IrP$_2$dppz** and **NiO**|**IrP$_4$dppz**, DAS(τ_1) and DAS(τ_2) show the same spectral shapes. The kinetic component associated with τ_1 (4.2 and 8.2 ps for **NiO**|**IrP$_2$dppz** and **NiO**|**IrP$_4$dppz**, respectively) shows a transient absorption decay at 460 nm, *i.e.* in the spectral region that has been previously associated with the reduced CN ligand. Hence, τ_1 reflects the geminate recombination of the electron residing on the reduced CN ligand and a hole injected into the NiO. The charge separated state, in which the electron resides on the dppz ligand is longer lived (due to a larger spatial separation between the hole and the electron) and decays with τ_2 (189 and 400 ps for **NiO**|**IrP$_2$dppz** and **NiO**|**IrP$_4$dppz**, respectively). The latter assignment is also based on the position of the ESA band indicated in DAS(τ_2). This assignment, which is in line with the results from spectroelectrochemistry (*vide supra*) implies that hole injection from the photoexcited Iridium(III) complexes to the NiO occurs ultrafast, *i.e.* faster than the time-resolution of our experiment. This ultrafast hole injection reflects the large injection driving force for hole injection as well as a strong electronic coupling between the excited photosensitizer and the NiO. Furthermore, this is in agreement with other literature reports on ultrafast hole injection in NiO based photocathodes.[35]

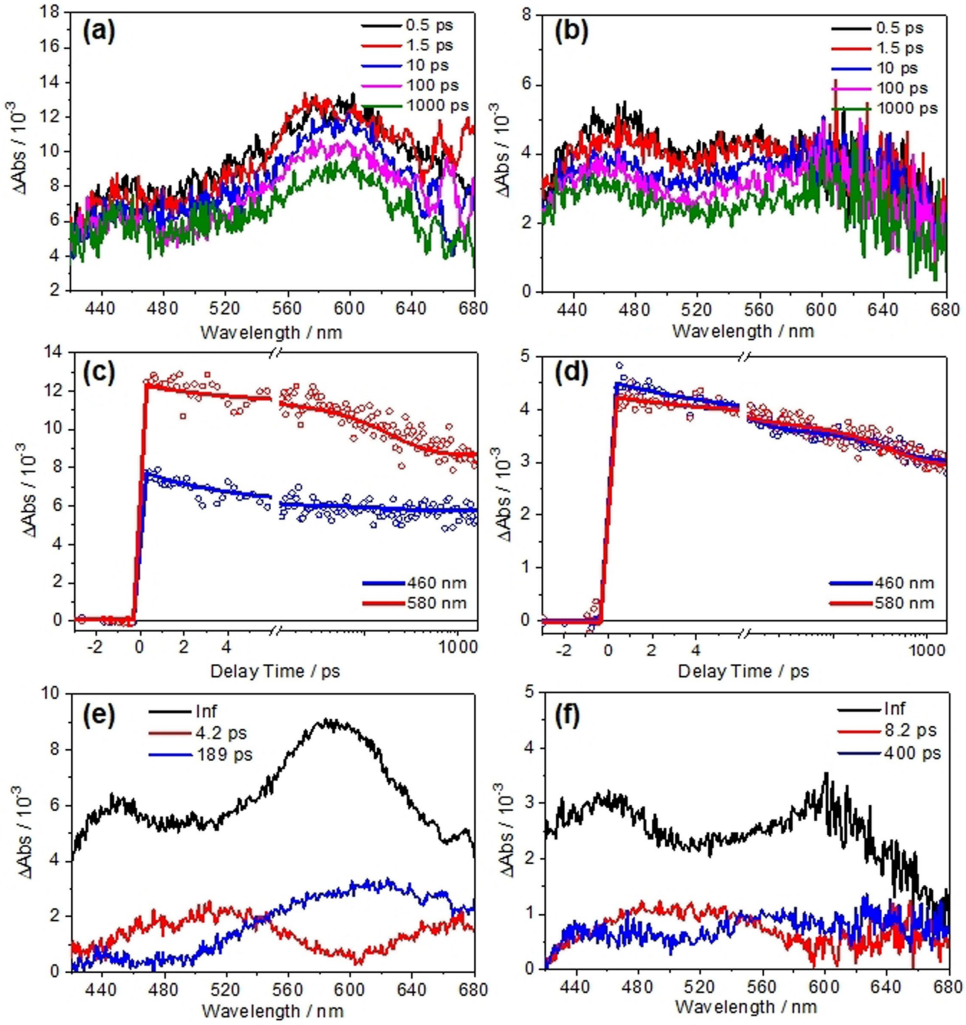

Figure 7. Transient absorption and the decay-associated spectra of (a,c) **NiO**|**IrP$_2$dppz** and (b,d) **NiO**|**IrP$_4$dppz** in contact with diluted I_3^-/I^- electrolyte in acetonitrile. The excitation wavelength was centered at 400 nm with power of 0.21 mW.

DAS(τ_3) reflects a decay of both ESA bands at 460 and 570 nm indicative of the reduced CN and reduced dppz ligands, respectively. The comparably slow kinetics suggest that the decay is due to non-geminate recombination of the charge-separated states, an effect that has been detailed by Hammarström and coworkers.[36a] Relating the initial amplitude of the transient absorption signal to the signal remaining at long delay times, it can be concluded that about 75% of the initially excited molecules populate a charge separated state, *i.e.* either h^+(NiO)|$CN^{\bullet-}$ or h^+(NiO)|$dppz^{\bullet-}$, irrespective of the sensitizer. Comparing the shape of the DAS(τ_3) for **NiO**|**IrP$_2$dppz** and **NiO**|**IrP$_4$dppz**, it is apparent that the ratio of band associated with the h^+(NiO)|$CN^{\bullet-}$ or h^+(NiO)|$dppz^{\bullet-}$ change. For **NiO**|**IrP$_2$dppz** the band intensity ratio is 2:3, while it is 1:1 for **NiO**|**IrP$_4$dppz**. This indicates a higher population in the h^+(NiO)|$dppz^{\bullet-}$ (compared to the population of the h^+(NiO)|$CN^{\bullet-}$) in **NiO**|**IrP$_2$dppz**. We refer this result to the increase in $LUMO^{dppz}$ energy upon adding the additional phosphonate anchoring groups. As the $LUMO^{dppz}$ energy in **IrP$_2$dppz** is lower than **IrP$_4$dppz**, localization of charge separated state on dppz ligand becomes more accessible after photoexcitation of **NiO**|**IrP$_2$dppz** than **NiO**|**IrP$_4$dppz**.

In addition to increasing the LUMO energy, extending the anchoring groups from two (**IrP$_2$dppz**) to four $-CH_2PO(OH)_2$ (**IrP$_4$dppz**) slows down the geminate recombination kinetics by roughly a factor of 2. We ascribe this hindered geminate recombination to the increased steric bulkiness of the anchoring group,[35b] likely hindering the reduced photosensitizer to efficiently fluctuate into geometries with efficient electronic coupling for charge recombination. Overall, the charge separation process including hole injection and recombination occurring at the Iridium(III) complexes|NiO interface is illustrated in Figure 8.

2.3. Dye-Sensitized Solar Cells

IrP$_2$dppz and **IrP$_4$dppz** have been tested as photosensitizers in p-DSSCs. The resultant J–V curves are shown in Figure 9a and the solar cell parameters are summarized in Table 3. To

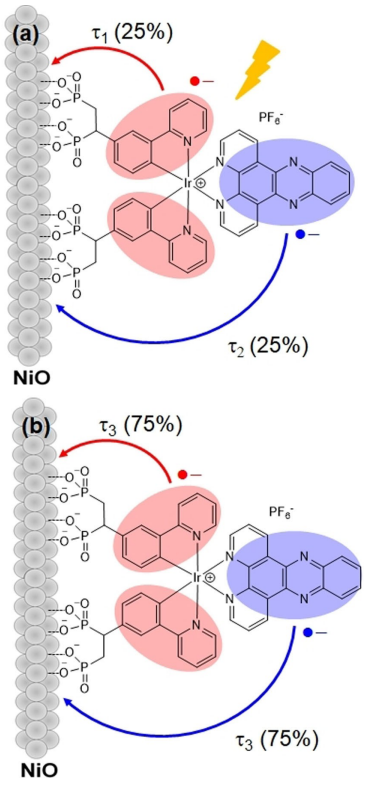

Figure 8. Schematic representation of the processes underlying (a) the fast and (b) the slow decay of h^+(NiO)/$CN^{\bullet-}$ and h^+(NiO)/$dppz^{\bullet-}$ CSS following photodriven hole injection from the excited Ir(III) photosensitizer to the valence band of NiO. The fast and slow decay of CSS amount to 25 and 75% of CSS signal, respectively.

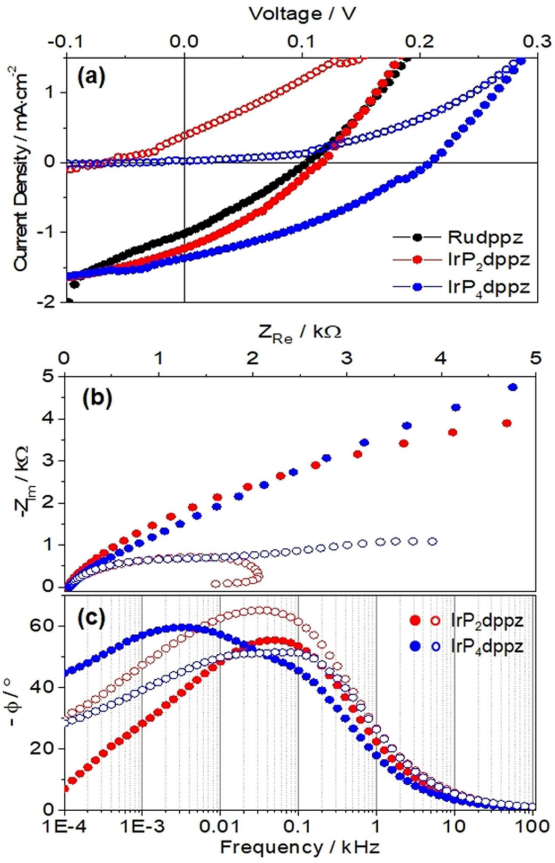

Figure 9. (a) Current-voltage curves and impedance data, including (b) Nyquist and (c) Bode plot, of p-DSSCs using **IrP_2dppz** and **IrP_4dppz** measured under dark (solid circles) and 100 mW·cm^{-2} solar simulator irradiation (empty circles). As comparison, a current-voltage curve for a p-DSSC using Rudppz complex is shown in panel (a).

benchmark the results, we compare the data to NiO cathodes sensitized with RuP_4dppz, *i.e.* ruthenium(II)(bis[4,4'-bis((methylene)phosphonicacid)-2,2′-bipyridine][dipyrido-phenazine]) $(PF_6)_2$, integrated into p-DSSCs. The Iridium(III) sensitizers yield higher short-circuit current densities (J_{sc}) than the Ru^{II} benchmark. **IrP_2dppz** and **IrP_4dppz** yield an average power conversion efficiency (η) of 0.034% and 0.078%, respectively. These values are superior to the efficiencies reported for Iridium(III) dppz sensitizers with –COOH anchoring groups (0.013%)[23] and represent (to the best of our knowledge) the highest efficiencies for NiO-based p-DSSCs using cyclometalated Iridium(III) complexes as sensitizers and an I_3^-/I^- redox shuttle.[21–23] The high photocurrent obtained here is due to comparably high dye-loading (Γ) of the electrodes, *i.e.* 6.4(±1.6)–11.3(±1.7) nmol·cm^{-2}, as compared to 1.8 (±0.1) nmol·cm^{-2} using the Ru-dppz complex. Despite the high power conversion efficiency and increased photocurrent, the molecular electron transfer at the **NiO**|**IrP_2dppz** and **NiO**|**IrP_4dppz** interfaces, which characterizes the net flow of electrons of sensitizer immobilized on the surface, is lower than in **NiO**|**Rudppz** (0.12–0.17 mA·$nmol^{-1}$ *vs* 0.49 mA·$nmol^{-1}$). The higher molecular electron transfer at **NiO**|**IrP_2dppz** compared to **NiO**|**IrP_4dppz** is rationalized by the transient absorption study, in which the longer-living h^+(NiO)|$dppz^{\bullet-}$ dominates the CSS rather than h^+(NiO)|$CN^{\bullet-}$.

Table 3. Solar cell parameters measured under 100 mWcm^{-2} solar simulator irradiation and electrochemical properties determined from electrochemical impedance spectroscopy.

Dye	V_{oc} [mV]	J_{sc} [mA·cm^{-2}]	FF	η [%]	Γ[a] [nmol·cm^{-2}]	R_{ct} [kΩ]	τ_h[b] [s]
IrP_2dppz	109	1.09	0.28	0.034	6.4	1.3	1.1
IrP_4dppz	209	1.13	0.33	0.078	11.3	4.1	0.7
RuP_4dppz	102	0.88	0.29	0.026	1.8	–	–

[a] Dye-loading (Γ) was estimated from the dye desorption test using 1 M NaOH solution in a water:ethanol mixture (1:1 v/v) for 2 h. [b] The hole lifetime (τ) is determined from the product of the chemical capacitance (C_μ) and the recombination resistance (R_{CT}).

The open circuit voltage (V_{oc}) of **NiO**|**IrP_4dppz** is two-fold higher than in **NiO**|**IrP_2dppz**. V_{oc} is proportional to the shunt resistance (R_{sh}) which predominantly stems from the recombination reaction at the NiO|dye|electrolyte interface.[37b,c] Therefore, electrochemical impedance spectroscopy (EIS) was carried out to unravel the charge transfer process across this interface. The resulting impedance data is shown in the Nyquist (Figure 10b) and Bode phase plot (Figure 10c). Upon irradiation the semicircle of Nyquist plot associated with the NiO|dye|electrolyte interface in the mid frequency region (10 to 500 Hz)

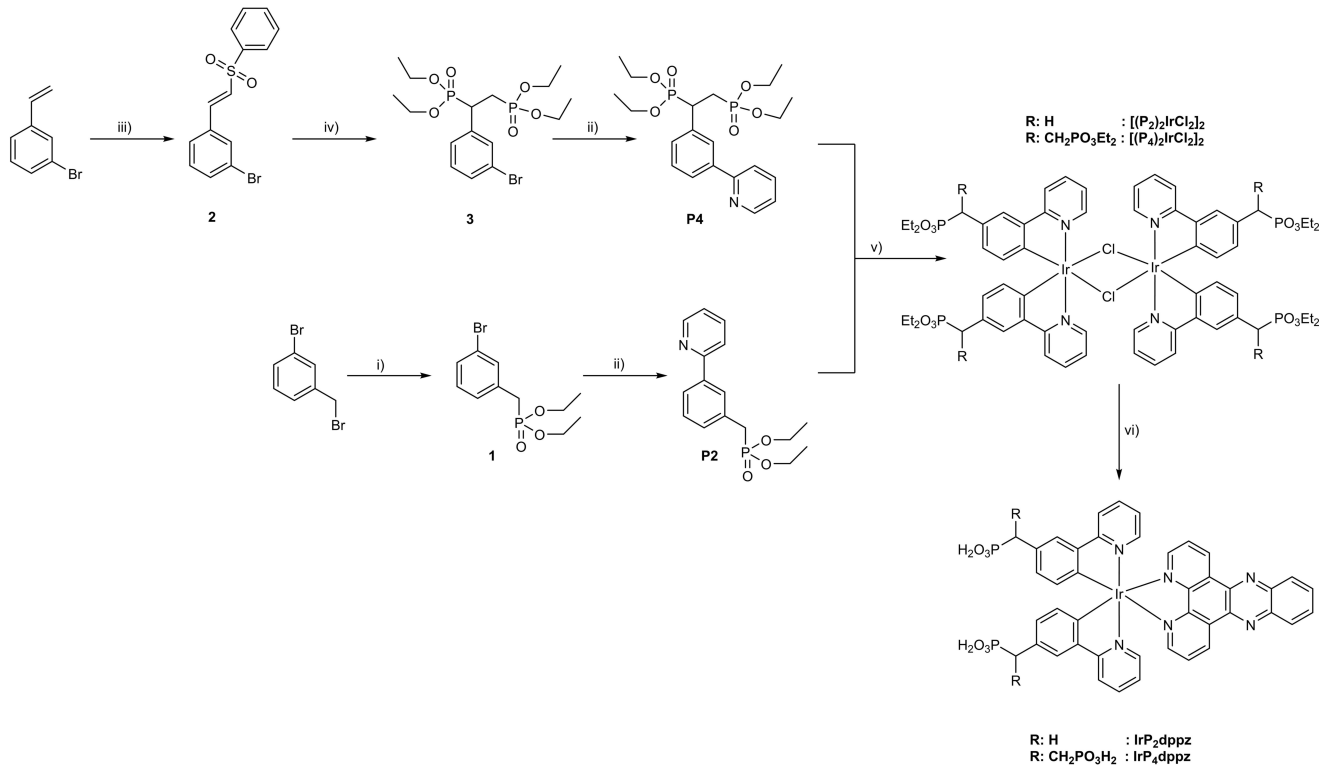

Figure 10. Synthetic scheme for the synthesis of **IrP$_2$dppz** and **IrP$_4$dppz**. i) PO_3Et_2, 80 °C, 12 h; ii) 2-(tributylstannyl)pyridine, $Pd(PPh_3)_4$, toluene, 120 °C, 48 h; iii) sodium benzenesulfinate, NaI, CAN, acetonitrile, r.t., 45 min; iv) KO^{t}Bu, $(H)OPO_2Et_2$, r.t., 45 min; v) $IrCl_3$, EtOEtOH, 3d, 130 °C; vi) dppz, CH_2Cl_2/EtOH, 2 h, 80 °C.

becomes smaller indicating additional charge flow across the interface due to charge injection from the photoexcited dye to NiO electrode. The impedance data was further fitted using the relevant equivalent circuit model[38] to extract relevant electrochemical parameters quantitatively (Table 3), such as charge recombination resistance (R_{ct}) and hole lifetime (τ_h) for interfacial recombination with the reduced species in electrolyte. The analysis reveals similar τ_h but different R_{ct} at the **NiO**|**IrP$_4$dppz**|**electrolyte** interface (4.3 kΩ), which is higher than that at the **NiO**|**IrP$_2$dppz**|**electrolyte** interface (1.3 kΩ). The higher R_{ct} is due to high NiO surface coverage (Γ) promoted by a more stable grafting at **NiO**|**IrP$_4$dppz**. Furthermore, higher Γ is advantageous for the cell performance since it shields the charge recombination reaction between either injected hole or non-geminate hole on NiO surface with the reduced species in the electrolyte (I^-).[25,37]

3. Conclusion

We have prepared cyclometalated Iridium(III) complexes with dppz ancillary ligands bearing two different anchoring groups as photosensitizers for NiO-based p-DSSC. The structural pattern of the anchoring ligand, *i. e.* from two (**IrP$_2$dppz**) to four $CH_2PO(OH)_2$ (**IrP$_4$dppz**), enables to tune the HOMO-LUMO gap and modifies the grafting properties of the complexes. Both complexes show potentially exergonic hole injection and dye regeneration, which is important for applications in p-DSSC. Transient absorption studies unravel the excited state dynamics of the complexes in solution as well as the excited state charge separation mechanism of the complexes immobilized on NiO. The long-lived charge separated state (CSS) character distinguishes the nature between both complexes upon grafting on NiO: h^+(NiO)|dppz$^{\bullet-}$ dominates the CSS at **NiO**|**IrP$_2$dppz** while h^+(NiO)|CN$^{\bullet-}$ dominates the CSS at **NiO**|**IrP$_4$dppz**. However, fast partial decay of the CSS on a few ps to hundreds ps timescale could limit the sensitizer's performance. Albeit their low absorptivity in the visible regime both complexes work as sensitizers in p-DSSCs with conversion efficiencies of up to 0.078% for **IrP$_4$dppz** due to its high grafting density on NiO.

Experimental Section

Synthesis of IrP$_2$dppz and IrP$_4$dppz

Ceric ammonium nitrate and sodium benzenesulfinate were purchased from Alfa Aesar. 1-bromo-3-vinylbenzene was purchased from ABCR. Triethyl phosphite and diethyl phosphite were purchased from Sigma-Aldrich. The synthesis of dppz **(dipyrido[3,2-a:2′,3′-c]phenazine)** is reported elsewhere.[39] ^{1}H (400-MHz), ^{13}C (101 MHz) and ^{31}P (162 MHz) NMR spectra were measured in $CDCl_3$ or CD_3OD with a Bruker DRX 400 spectrometer at 298 K. The spectra were referenced to the solvent peak of chloroform ($\delta =$ 7.260 ppm) or methanol ($\delta = 4.870$ ppm). MS analysis was performed on Bruker solariX (2010) Hybrid 7 T FT-ICR for MALDI, ESI and APCI. The procedure for the synthesis of **IrP$_2$dppz** and **IrP$_4$dppz** is shown in Figure 10. Ligand **P2** can be synthesized starting from1-bromo-3-(bromomethyl)benzene. The introduction of the phosphonate was conducted by nucleophilic substitution

and subsequent Stille-coupling with 2-(tributylstannyl)pyridine. **P4** was synthesized starting from 1-bromo-3-vinylbenzene. The introduction of the phosphonate involved vinylic substitution and subsequent addition. Stille coupling with 2-(tributylstannyl)pyridine led to **P4**. Both ligands were introduced to $IrCl_3$ in 2-ethoxyethan-1-ol at high temperature to form the corresponding dimers $(\mathbf{P_2})_2\mathbf{IrCl_2}$ and $(\mathbf{(P_4)_2IrCl_2}$. It has to be noted, that for **P2** these conditions lead to a loss of one or more ethyl groups on the phosphonates. The dimers were than reacted with dppz in a mixture of dichloromethane and ethanol to form the diethyl phosphonate complexes $\mathbf{IrP_2dppz^{Et}}$ and $\mathbf{IrP_4dppz^{Et}}$. Only small amounts of the diethyl phosphonate compound $\mathbf{IrP_2dppz^{Et}}$ could be isolated and were used for the electrochemical characterization. Surprisingly the loss of ethyl groups was not present in **P4**, therefore $\mathbf{IrP_4dppz^{Et}}$ could be isolated. $\mathbf{IrP_2dppz^{Et}}$ and $\mathbf{IrP_4dppz^{Et}}$ were subsequently deprotected using TMSBr to form the free phosphonic acid $\mathbf{IrP_2dppz}$ and $\mathbf{IrP_4dppz}$. Due to the chiral character of ligand **P4** and the Δ,Λ-isomerism in $\mathbf{IrP_4dppz^{Et}}$ and $\mathbf{IrP_4dppz}$, the ^{1}H– as well as the ^{31}P-NMR spectra are very complicated. Especially the ^{1}H-NMR is hard to interpret in the aliphatic region (SI, Figure S19).

Diethyl (3-bromobenzyl)phosphonate (1)

A mixture of 1-bromo-3-(bromomethyl)benzene (1 g, 4 mmol) and triethyl phosphite (8.6 mL, 50 mmol) was heated to 100 °C for 12 h. Triethyl phosphite was removed under reduced pressure and **1** could be isolated as a colorless oil in quantitative yield.

^{1}H NMR (400 MHz, $CDCl_3$) δ 7.42 (dtd, J = 2.5, 2.1, 0.4 Hz, 1H), 7.38–7.34 (m, 1H), 7.24–7.20 (m, 1H), 7.19–7.13 (m, 1H), 4.06–3.96 (m, 4H), 3.09 (d, J = 21.7 Hz, 2H), 1.27–1.20 (m, 6H).

^{31}P NMR (162 MHz, $CDCl_3$) δ 26.65.

Diethyl (3-(pyridin-2-yl)benzyl)phosphonate (P2)

A solution of **1** (0.5 g, 1.6 mmol) in toluene (15 mL) was degassed with Argon. To the solution 2-(tributylstannyl)pyridine (0.72 mL, 2 mmol) and $Pd(PPh_3)_4$ (0.2 g, 0.2 mmol) were added under an Argon flow. The mixture was heated to reflux for 48 h under an Argon atmosphere. After that time the solvent was evaporated under reduced pressure and the crude product was purified using column chromatography (silica, EtOAc/MeOH, 8/1, v/v). The so obtained yellow oil was taken up in n-hexane and the solid was filtered off. After evaporation of the solvent **P2** could be obtained as off-white oil (263 mg, 53 %).

^{1}H NMR (400 MHz, $CDCl_3$) δ 8.70–8.56 (m, 1H), 7.90 (dt, J = 1.8, 1.2 Hz, 1H), 7.84 (ddd, J = 7.6, 3.6, 1.8 Hz, 1H), 7.71–7.69 (m, 1H), 7.69 (d, J = 1.4 Hz, 1H), 7.41–7.36 (m, 1H), 7.36–7.31 (m, 1H), 7.18 (ddd, J = 5.3, 4.8, 3.2 Hz, 1H), 4.05–3.87 (m, 4H), 3.21 (d, J = 21.6 Hz, 2H), 1.27–1.14 (m, 6H).

^{31}P NMR (162 MHz, $CDCl_3$) δ 27.48.

HRMS (ESI, acetonitrile): $C_{16}H_{20}NO_3P$ calc. 306.12536; found 306.12468 $[M]^+$.

1-Bromo-3-(2-(phenylsulfonyl)vinyl)benzene (2)

2 was synthesized by a literature known procedure.[40] 1-bromo-3-vinylbenzene (0.5 g, 2.76 mmol), sodium benzenesulfinate (0.68 g, 4.14 mmol) and NaI (0.62 g, 4.14 mmol) were added to a Schlenk flask and acetonitrile (36 mL) was added. The mixture was degassed with argon. A solution of Ceric ammonium nitrate (3.5 g, 6.35 mmol) in acetonitrile (24 mL) was degassed with argon and added to the mixture in the course of 45 min. After that time the solvent was removed under reduced pressure. The crude product was diluted with water and extracted with dichloromethane. The organic layer was washed with water, saturated sodium thiosulfate solution and brine. After recrystallized from n-hexane the product could be isolated as an off white solid (480 mg, 54 %).

^{1}H NMR (400 MHz, $CDCl_3$) δ 7.95 (d, J = 7.2 Hz, 2H), 7.64–7.53 (m, 6H), 7.41 (d, J = 7.9 Hz, 1H), 7.28 (d, J = 8.0 Hz, 1H), 6.87 (d, J = 15.4 Hz, 1H).

HRMS (APCI): $C_{14}H_{12}BrO_2S$ calc.322.9741; found 322.9746 $[M+H^+]^+$.

Tetraethyl (1-(3-bromophenyl)ethane-1,2-diyl)bis (phosphonate) (3)

3 was prepared using a literature known procedure.[41] A degassed mixture of diethyl phosphite (3.2 g, 23 mmol) and Potassium *tert*-butoxide (505 mg, 4.5 mmol) was added to **2** (0.48 g, 1.5 mmol). Upon addition the instantaneously formed solution turned yellow. The mixture was stirred under Argon at r.t. for 45 min. After that time water was added and the aqueous solution was extracted with diethyl ether. The combined organic layers were dried over Magnesium sulfate and evaporated to dryness to yield **4** as off white oil (393 mg, 57 %).

^{31}P NMR (162 MHz, $CDCl_3$) δ 27.93 (d, J = 80.7 Hz), 26.12 (d, J = 80.7 Hz).

HRMS (APCI): $C_{16}H_{27}BrO_6P_2$ calc. 457.0539; found 457.0539 $[M+H^+]^+$.

Tetraethyl (1-(3-(pyridin-2-yl)phenyl)ethane-1,2-diyl)bis (phosphonate) (P4)

A solution of **3** (0.37 g, 0.81 mmol) in toluene (15 mL) was degassed with Argon. To the solution 2-(tributylstannyl)pyridine (0.37 mL, 1.01 mmol) and $Pd(PPh_3)_4$ (0.05 g, 40.50 μmol) were added under an Argon flow. The mixture was heated to reflux for 48 h under an Argon atmosphere. After that time the solvent was evaporated under reduced pressure and the crude product was purified using column chromatography (silica, EtOAc to EtOAc/MeOH, 8/1, v/v). $\mathbf{P_4}$ could be obtained as a colorless oil (62 mg, 17 %).

^{1}H NMR (400 MHz, CDCl3) δ 8.72 (s, 1H), 8.01 (s, 1H), 7.82 (s, 1H), 7.72–7.58 (m, 1H), 7.56–7.41 (m, 2H), 7.40–7.28 (m, 1H), 4.16–3.52 (m, 9), 2.55–2.50 (m, 2H), 1.35–1.00 (m, 12H).

^{31}P NMR (162 MHz, $CDCl_3$) δ 28.46 (d, J = 81.5 Hz), 26.90 (d, J = 81.5 Hz).

HRMS (MADLI): $C_{21}H_{32}NO_6P_2$ calc. 456.17049; found 456.16947 $[M+H^+]^+$; $C_{21}H_{31}NNaO_6P_2$ calc. 478.15243; found 478.15125 $[M+Na^+]^+$; $C_{27}H_{40}N_4NaO_6P_2$ calc. 601.23153; found 601.16363 $[M+3\ ACN+Na^+]^+$.

Dichlorotetrakis[diethyl (3-(pyridin-2-yl)benzyl) phosphonate]-diiridium(III) $(\mathbf{(P_2)_2IrCl_2})$

A mixture of $IrCl_3 \cdot xH_2O$ (0.170 g, 0.56 mmol) and $\mathbf{P_2}$ (0.08 g, 0.28 mmol) in 2-ethoxyethanol/water (4.50 mL, 3/1, v/v) was heated to 130 °C for 3 days under an Argon atmosphere. After that time water (20 mL) was added and the yellow precipitate was filtered off (131 mg, 56 %).

^{1}H NMR (400 MHz, $CDCl_3$) δ 9.21 (d, J = 5.1 Hz, 4H), 7.89 (d, J = 7.5 Hz, 4H), 7.78–7.68 (m, 4H), 7.50–7.45 (m, 4H), 6.78 (t, J = 5.9 Hz, 4H), 6.47 (d, J = 8.1 Hz, 4H), 5.80 (d, J = 7.5 Hz, 4H), 3.95–3.74 (m, 16H), 2.92 (dd, J = 21.0, 2.9 Hz, 8H), 1.11 (dd, J = 13.3, 7.0 Hz, 24H).

^{31}P NMR (162 MHz, $CDCl_3$) δ 26.84.

[$(P_2)_2$Ir(dppz)](PF_6) (IrP_2dppz)

A solution of dppz (0.024 g, 0.084 mmol) in a 4 mL mixture of dichloromethane/ethanol (3/1, v/v) was added to a solution of (($(P_2)_2IrCl_2$) (0.071 g, 0.042 mmol) in 8 mL of the same solvent. The mixture was heated to reflux for 2 h, after that time the color changed from yellow to orange. The dichloromethane was removed in vacuum and the product was precipitated by addition of aqueous NH_4PF_6 (20 eq). The solid was filtered off and washed with Et_2O. The raw product was a mixture of ethyl phosphonate and the free phosphonic acid. A small amount of the diethyl phosphonate compound (IrP_2dppz^{Et}) could be isolated, which was used for the electrochemical characterization, but it was decided to deprotect the compound directly to simplify purification and characterization. Therefore, the crude product was dissolved in dichloromethane (10 mL) and was directly deprotected using trimethylsilyl bromide (100 eq). After addition of methanol und removal of the solvent in vacuum **P_2Irdppz** was obtained as a yellow powder (55 mg, 72%).

^{1}H NMR (400 MHz, $CDCl_3$) δ 9.66 (dd, J = 8.3, 1.5 Hz, 2H), 8.37–8.20 (m, 4H), 7.93–7.88 (m, 4H), 7.84 (dd, J = 8.3, 5.2 Hz, 2H), 7.63–7.60 (m, 2H), 7.56–7.49 (m, 2H), 7.24 (d, J = 4.9 Hz, 2H), 6.75 (d, J = 7.8 Hz, 2H), 6.69–6.62 (m, 2H), 6.05 (d, J = 7.7 Hz, 2H), 2.74 (d, J = 20.4 Hz, 4H).

^{31}P NMR (162 MHz, $CDCl_3$) δ 22.93.

HRMS (ESI, acetonitrile): $C_{42}H_{32}IrN_6O_6P_2$ calc. 971.14849; found 971.14849. $[M]^+$.

Dichlorotetrakis[tetraethyl (1-(3-(pyridin-2-yl)phenyl) ethane-1,2-diyl)bis(phosphonate)]-diiridium(III) (($(P_4)_2IrCl_2$)

A mixture of $IrCl_3 \cdot xH_2O$ (0.062 g, 0.136 mmol) and **P_4** (0.020 g, 0.068 mmol) in 2-ethoxyethanol/water (7 mL, 3/1, v/v) was heated to 130 °C for 3 days under an Argon atmosphere. After that time the solvent was removed under vacuum and the residue was dissolved in a minimum amount of $CHCl_3$. After addition of Et_2O the product could be filtered off as yellow solid. (82 mg, 56%).

^{31}P NMR (162 MHz, CDCl3) δ 31.89 (d, J = 81.4 Hz), 29.94 (d, J = 81.4 Hz).

[(P_4^{Et})$_2$Ir(dppz)](PF_6) (IrP_4dppz^{Et})

A solution of dppz (0.020 g, 0.072 mmol) in a 2 mL mixture of chloroform/ethanol (3/1, v/v) was added to a solution of (($(P_4)_2IrCl_2$) (0.082 g, 0.038 mmol) in 9 mL of the same solvent. The mixture was heated to 80 °C for 2 h and stirred at r.t. for 12 h. After that time the color changed from yellow to orange. The solvent was removed in vacuum and the product was precipitated by addition of aqueous NH_4PF_6 (20 eq). The crude product was purified by size exclusion chromatography (sephadex LH-20, chloroform/methanol/acetone, 3/3/4, v/v) to yield the diethyl phosphonate compound (IrP_4dppz^{Et}) as an orange powder (77 mg, 75%).

^{1}H NMR (400 MHz, $CDCl_3$) δ 10.25–10.22 (m, 1H), 9.92–9.77 (m, 2H), 9.45 (dd, J = 18.1, 4.9 Hz, 2H), 8.58 (t, J = 8.1 Hz, 1H), 8.51–8.27 (m, 4H), 8.16–7.64 (m, 7H), 7.64–7.38 (m, 4H), 6.99 (d, J = 4.4 Hz, 1H), 6.68 (dd, J = 6.5, 5.1 Hz, 1H), 6.39 (dd, J = 10.2, 2.5 Hz, 1H), 4.29–3.58 (m, 16H), 2.68–2.45 (m, 6H), 1.50–1.09 (m, 24H).

31P NMR (162 MHz, CDCl3) δ 28.53–27.83 (m).

HRMS (MALDI): $C_{60}H_{70}IrN_6O_{12}P_4$ calc. 1383.3631; found 1383.3629 $[M]^+$.

^{13}C NMR (126 MHz, CDCl3) δ 169.62, 167.29, 156.05, 155.72, 152.84, 152.21, 151.35, 150.09, 149.88, 149.38, 148.63, 143.28, 139.71, 138.54, 137.87, 136.22, 135.95, 135.28, 133.84, 132.30, 131.49, 130.44, 129.41, 128.15, 127.62, 126.63, 126.43, 126.00, 124.96, 124.30, 122.41, 120.03, 119.57, 63.32, 62.47, 61.86, 39.38, 38.33, 29.83.

[(P_4)$_2$Ir(dppz)](PF_6) (IrP_4dppz)

IrP_4dppz^{Et} was dissolved in dichloromethane and trimethylsilyl bromide (100 eq.) was added. The solution was stirred for 12 h and methanol was added to the solution. After removal of the solvent, the crude product was purified by diffusion of diethyl ether into a methanol solution of **IrP_4dppz**

^{31}P NMR (162 MHz, MeOD) δ 26.96 (d, J = 63.7 Hz), 25.30 (d, J = 63.2 Hz).

Electrochemical and UV/vis Spectroelectrochemical Measurements

UV/Vis absorption and emission spectra were measured using a Varian-Cary UV-vis-NIR spectrometer and FLS980 photoluminescence spectrometer (Edinburg Instrument), respectively. The cyclic voltammetry of **IrP_2dppz** and **IrP_4dppz** was measured on a Gamry Interface 1010b Potentiostat/Galvanostat/ZRA with a glassy carbon working electrode and a Pt-wire counter electrode in a temperature-controlled cell under a constant Argon flow. For **IrP_2dppz** and **IrP_4dppz** the corresponding ethyl ester was used for solubility reasons. The dye was dissolved in ACN and the solution was degassed with argon. $TBAPF_6$ (0.1 M) was added as the supporting electrolyte. The CVs were taken at a scan rate of 100 mV/s at 25 °C. Spectroelectrochemical data was obtained by using a thin-layer quartz glass spectroelectrochemical cell (1 mm path length, Bioanalytical Systems, Inc.), equipped with a platinum counter electrode, a Ag|AgCl-pseudoreference electrode and a glassy carbon working electrode with a slit of 2 mm × 5 mm. UV/vis spectra were collected during reduction of the complexes, *i.e.* during chronoamperometry at various potentials. The UV/vis spectra were obtained in transmission mode through the slit of the glassy carbon working electrode using a single channel fiber optic spectrometer (Avantes Inc., AvaSpec-ULS2048XL) with a deuterium-halogen light source (Avantes Inc., AvaLight DH-S-BAL).

Time-Resolved Emission and Transient Absorption Measurements

Time-resolved emission measurements were carried out by using time-correlated single-photon counting (TCSPC).[9] A Ti:Sapphire laser (Tsunami, Newport Spectra-Physics GmbH) was used as the light source. The repetition rate is reduced to 400 kHz by a pulse selector (model 3980, Newport Spectra-Physics GmbH). Afterwards, the fundamental beam of the Ti-Sapphire oscillator is frequency doubled in a second harmonic generator (Newport Spectra-Physics GmbH) to create the 390-nm pump beam. The emission was detected by a Becker & Hickl PMC-100-4 photon-counting module. The emission lifetimes were determined by fitting a monoexponential-decay to the data. The set up for transient absorption measurements of **IrP_2dppz** and **IrP_4dppz** both in solutions and on NiO films was the following:[9,11,42] Pump pulses exciting the sample were centered at 400 nm with a pump-pulse energy of typically 1.2 μJ, while typical probe intensities fall into the range of hundred nJ. The mutual polarizations of pump and probe were set to magic

angle. Chirp correction and subsequently a global fit routine using a sum of exponentials was carried out for data analysis. To avoid prominent contributions from coherent artifacts,[43] the pulse overlap region (±250 fs around time zero) was excluded from the data fitting procedure.

DSSC Fabrication and Characterization

NiO-based DSSCs with typical area of 0.2 cm^2 were fabricated by sandwiching dye-sensitized NiO into a cell with platinized FTO as counter electrode. The dye sensitization was carried out by soaking the NiO film in 0.5 mM dye solution: A mixture of H_2O/ACN (1 : 9 v/v) was used as **IrP_2dppz** and **IrP_4dppz** solvent. A liquid electrolyte of I_3^-/I^- containing 0.5 M tetrabutylammonium iodide, 0.1 M lithium iodide, 0.1 M iodine and 0.5 M 4-*tert*-butylpyridine was used as redox mediator. Platinized FTO was used as the counter electrode and prepared according to literature. The amount of dye loading on the NiO photocathode was estimated by immersing the NiO photocathode in a 1 M NaOH solution in a water:ethanol mixture (1 : 1 v/v) for 2 h, resulting in the desorption of the dye molecules. The absorbance of the desorbed dye solution was measured and the amount of desorbed dye was determined by comparing the absorbance of the desorbed solution at the absorption maximum with the absorbance of a known concentration of the dye in 1 M NaOH solution with water and ethanol mixture (1 : 1 v/v). The current density-voltage (*J–V*) curves of DSSCs were measured under 100 mW cm^{-2} illumination using a solar simulator (SS-80 PET) with an AM1.5G reference spectrum. Electrochemical impedance spectroscopy was performed with a computer-controlled potentiostat (Princeton Applied Research VersaSTAT MC potentiostat) equipped with a frequency response analyzer. All impedance measurements were carried out both under bias illumination from a xenon light source and under dark condition. The obtained spectra were fitted with Z-View (v3.2c, Scribner Associate, Inc.) using established equivalent circuits.

Acknowledgements

This work was funded by the Deutsche Forschungsgemeinschaft (DFG, German Research Foundation) – project number 364549901-TRR 234 (CataLight Project A1). Financial support by the Deutscher Akademischer Austauschdienst (DAAD) for PhD Scholarship for RAW is gratefully acknowledged.

Conflict of Interest

The authors declare no conflict of interest.

Keywords: cyclometalation · dye-sensitized solar cells · electron transfer · iridium · photocathode · nickel oxide

[1] a) F. Odobel, Y. Pellegrin, E. A. Gibson, A. Hagfeldt, A. L. Smeigh, L. Hammarström, *Coord. Chem. Rev.* **2012**, *256*, 2414–2423; b) A. Nattestad, A. J. Mozer, M. K. R. Fischer, Y.-B. Cheng, A. Mishra, P. Bäuerle, U. Bach, *Nature Mat.* **2010**, *9*, 31–35; c) C. J. Wood, G. H. Summers, C. A. Clark, N. Kaeffer, M. Braeutigam, L. R. Carbone, L. D'Amario, K. Fan, Y. Farré, S. Narbey, F. Oswald, L. A. Stevens, C. D. J. parmenter, M. W. Fay, A. L. Torre, C. E. Snape, B. Dietzek, D. Dini, L. Hammarström, Y. Pellegrin, F. Odobel, L. Sun, V. Artero, E. A. Gibson, *Phys. Chem. Chem. Phys.* **2016**, *18*, 10727–10738.
[2] V. Nikolaou, A. Charisiadis, G. Charalambidis, A. G. Coutsolelos, F. Odobel, *J. Mater. Chem. A* **2017**, *5*, 2107.
[3] I. R. Perera, T. Daeneke, S. Makuta, Z. Yu, Y. Tachibana, A. Mishra, P. Bäuerle, C. A. Ohlin, U. Bach, L. Spiccia, *Angew. Chem. Int. Ed.* **2015**, *54*, 3758–3762.
[4] a) F. Odobel, Y. Pellegrin, *J. Phys. Chem. Lett.* **2013**, *4*, 2551–2564; b) Z. Yu, F. Li, L. Sun, *Energy Environ. Sci.* **2015**, *8*, 760–775.
[5] a) E. Benazzi, J. Mallows, G. H. Summers, F. A. Black, E. A. Gibson, *J. Mater. Chem. C* **2019**, *7*, 10409; b) E. A. Gibson, *Chem. Soc. Rev.* **2017**, *46*, 6194–6209.
[6] P. Qin, H. Zhu, T. Edvinsson, G. Boschloo, A. Hagfeldt, L. Sun, *J. Am. Chem. Soc.* **2008**, *130*, 8570–857.
[7] T. Marinado, K. Nonomura, J. Nissfolk, M. K. Karlsson, D. P. Hagberg, L. Sun, S. Mori, A. Hagfeldt, *Langmuir* **2010**, *26*, 2592–2598.
[8] L. Li, L. Duan, F. Wen, C. Li, M. Wang, A. Hagfeldt, L. Sun, *Chem. Commun.* **2012**, *48*, 988–990.
[9] M. Bräutigam, J. Kübel, M. Schulz, J. G. Vos, B. Dietzek, *Phys. Chem. Chem. Phys.* **2015**, *17*, 7823–7830.
[10] Y. Han, R. J. Dillon, C. J. Flynn, E. S. Rountree, L. Alibabaei, J. F. Cahoon, J. M. Papanikolas, J. L. Dempsey, *Can. J. Chem.* **2018**, *96*, 865–874.
[11] N. Queyriaux, R. A. Wahyuono, J. Fize, C. Gablin, M. Wächtler, E. Martinez, D. Leonard, B. Dietzek, V. Artero, M. Chavarot-Kerlidou, *J. Phys. Chem. C* **2017**, *121* (11), 5891–5904.
[12] Z. Ji, M. He, Z. Huang, U. Ozkan, Y. Wu, *J. Am. Chem. Soc.* **2013**, *135*(52), 11696–11699.
[13] Z. Ji, Y. Wu, *J. Phys. Chem. C* **2013**, *117*, 18315–18324.
[14] Z. Ji, G. Natu, Y. Wu, *Appl. Mater. Interfaces* **2013**, *5*(17), 8641–8648.
[15] Z. Ji, G. Natu, Z. Huang, O. Kokhan, X. Zhang, Y. Wu, *J. Phys. Chem. C* **2012**, *116*, 16854–16863.
[16] N. Marinakis, C. Wobill, E. C. Constable, C. E. Housecroft, *Polyhedron* **2018**, *140*, 122–128.
[17] a) P. G. Bomben, K. C. D. Robson, P. A. Sedach, C. P. Berlinguette, *Inorg. Chem.* **2009**, *48*, 9631–9643; b) P. G. Bomben, K. D. Thériault, C. P. Berlinguette, *Eur. J. Inorg. Chem.* **2011**, *111*, 2827–2829.
[18] Y. Pellegrin, L. Le Pleux, E. Blart, A. Renaud, B. Chavillon, N. Szuwarski, M. Boujtita, L. Cario, S. Jobic, D. Jacquemin, F. Odobel, *J. Photochem. Photobiol. A* **2011**, *219*, 235–242.
[19] B. Geiß, C. Lambert, *Chem. Commun.* **2009**, 1670–1672.
[20] L. Flamigni, A. Barbieri, C. Sabatini, B. Ventura, F. Barigelletti, *Top. Curr. Chem.* **2007**, *281*, 143–203.
[21] a) Hierlinger, H. V. Flint, D. B. Cordes, A. M. Z. Slawin, E. A. Gibson, D. Jacquemin, V. Guerchais, E. Zysman-Colman, *Polyhedron* **2018**, *140*, 109–115; b) F. Légalite, D. Escuerdo, Y. Pellegrin, E. Blart, D. Jacquemin, F. Odobel, *Dyes Pigm.* **2019**, *171*, 107693.
[22] A. Sinopoli, C. J. Wood, E. A. Gibson, P. I. P. Elliott, *Eur. J. Inorg. Chem.* **2016**, 2887–2890.
[23] A. Sinopoli, C. J. Wood, E. A. Gibson, P. I. P. Elliott, *Dyes Pigm.* **2017**, *140*, 269–277.
[24] D. D. Wang, H. Dong, Y. Wu, Y. Yu, G. Zhou, L. Li, Z. Wu, M. Gao, G. Wang, *J. Organomet. Chem.* **2015**, *775*, 55–59.
[25] M. Gennari, F. Légalité, L. Zhang, Y. Pellegrin, E. Blart, J. Fortage, A. M. brown, A. Deronzier, M.-N. Collomb, M. Boujtita, D. Jacquemin, L. Hammarström, F. Odobel, *J. Phys. Chem. Lett.* **2014**, *5*, 2254–2258.
[26] a) L. Zhang, J. M. Cole, *ACS Appl. Mater. Interfaces* **2015**, *7*, 3427–3455; b) A. Hagfeldt, G. Boschloo, L. Sun, L. Kloo, H. Pettersson, *Chem. Rev.* **2010**, *110*, 6595–6663; c) G. Deacon, *Coord. Chem. Rev.* **1980**, *33*, 227–250.
[27] C. She, J. Guo, S. irle, K. Morokuma, D. L. Mohler, H. Zabri, F. odobel, K.-T. Youm, F. Liu, J. T. Hupp, T. Lian, *J. Phys. Chem. A* **2007**, *111*, 6832–6842.
[28] a) M. G. Pfeffer, B. Schäfer, G. Smolentsev, J. Uhlig, E. Nazarenko, J. Guthmuller, C. Kuhnt, M. Wächtler, B. Dietzek, V. Sundström, S. Rau, *Angew. Chem. Int. Ed.* **2015**, *54*(17), 5044–5048; b) M. G. Pfeffer, T. Kowacs, M. Wächtler, J. Guthmuller, B. Dietzek, J. G. Vos, S. Rau, *Angew. Chem.* **2015**, *54*(22), 6627–6631.
[29] a) A. M. Brouwer, *Pure Appl. Chem.* **2011**, *83*, 2213; b) G. Boschloo, A. Hagfeldt, *Acc. Chem. Res.* **2009**, *42*, 1819–1826; c) V. Pavlishchuk, A. W. Addison, *Inorg. Chim. Acta* **2000**, *298*, 97–102.
[30] a) R. Luschtinetz, G. Seifert, E. Jaehne, H.-J. P. Adler, *Macromol. Symp.* **2007**, *254*, 248–253; b) M. C. Zenobi, C. V. Luengo, M. J. Avena, E. H. Rueda, *Spectrochim. Acta Part A* **2008**, *70*, 270–276.
[31] a) A. W. McKinley, P. Lincoln, E. M. Tuite, *Coord. Chem. Rev.* **2011**, *255*, 2676–2692; b) J. Olofsson, B. Önfelt, P. Lincoln, *J. Phys. Chem. A* **2004**,

108, 4391–4398; c) Y. Sun, S. N. Collins, L. E. Joyce, C. Turro, *Inorg. Chem.* **2010**, *49*, 4257–4562.
[32] a) K. W. Lee, J. D. Slinker, A. A. Gorodetsky, S. Flores-Torres, H. D. Abruna, P. L. Houston, G. G. Malliaras, *Phys. Chem. Chem. Phys.* **2003**, *5*, 2706–2709; b) L. Dennany, T. E. Keyes, R. J. Forster, *Analyst* **2008**,*133*, 753–755.
[33] a) S. Tschierlei, A. Neubauer, N. Rockstroh, M. Karnahl, P. Schwarzbach, H. Junge, M. Beller, S. Lochbrunner, *Phys. Chem. Chem. Phys.* **2016**, *18*, 10682; b) S. Tschierlei, M. Presselt, C. Kuhnt, A. Yartsev, T. Pascher, V. Sundström, M. Karnahl, M. Schwalbe, B. Schäfer, S. Rau, M. Schmitt, B. Dietzek, J. Popp, *Chem. Eur. J.* **2009**, *15*, 7678; c) C. Kuhnt, M. Karnahl, S. Tschierlei, K. Griebenow, M. Schmitt, B. Schäfer, S. Krieck, H. Görls, S. Rau, B. Dietzek, J. Popp, *Phys. Chem. Chem. Phys.* **2010**, *12*, 1357–1368; d) M. G. Pfeffer, B. Schäfer, G. Smolentsev, J. Uhlig, E. Nazarenko, H. Guthmuller, C. Kuhnt, M. Wächtler, B. Dietzek, V. Sundström, S. Rau, *Angew. Chem. Int. Ed.* **2015**, *54*, 5044; e) J. F. Levebvre, J. Schindler, P. Traber, Y. Zhang, S. Kupfer, S. Gräfe, I. Baussanne, M. Demeunynck, J. M. Mouesca, S. Gambarelli, V. Artero, B. Dietzek, M. Chavarot-Kerlidou, *Chem. Sci.* **2018**, *9*, 4152–4159.
[34] E. J. C. Olson, D. Hu, A. Hörmann, A. M. Jonkman, M. R. Arkin, E. D. A. Stemp, J. K. Barton, P. F. Barbara, *J. Am. Chem. Soc.* **1997**, *119*, 47, 11458–11467.
[35] a) A. M. Brown, L. J. Antila, M. Mirmohades, S. Pullen, S. Ott, L. Hammarström, *J. Am. Chem. Soc.* **2016**, *138*, 8060–8063; b) A. Morandeira, G. Boschloo, A. Hagfeldt, L. Hammarström, *J. Phys. Chem. B* **2005**, *109*, 19403–19410; c) J. Warnan, Y. Pellegrin, E. Blart, L. Zhang, A. Brown, L. Hammarström, D. Jacquemin, F. Odobel, *Dyes Pigm.* **2014**, *105*, 174–179; d) A. Morandeira, G. Boschloo, A. Hagfeldt, L. Hammarström, *J. Phys. Chem. C* **2008**, *112*, 9530–9537.
[36] a) L. D'Amario, L. J. Antila, B. P. Rimgard, G. Boschloo, L. Hammarström, *J. Phys. Chem. Lett.* **2015**, *6*, 779–783; b) A. Kobayashi, S. Watanabe, M. Ebina, M. Yoshida, M. Kato, *J. Photochem. Photobiol. A* 2017, 347, 9–16.
[37] a) S. R. Raga, E. M. Barea, F. Fabregat-Santiago, *J. Phys. Chem. Lett.* **2012**, *3*, 1629–1634; b) N. Koide, A. Islam, Y. Chiba, L. Han, *J. Photochem. Photobiol. A* **2006**, *182*, 296–395; c) S. Rühle, M. Greenshtein, S. G. Chen, A. Merson, H. Pizem, C. S. Sukenik, D. Cahen, A. Zaban, *J. Phys. Chem. B* **2005**, *109*, 18907–18913.
[38] a) Z. Huang, G. Natu, Z. Ji, P. Hasin, Y. Wu, *J. Phys. Chem. C* **2011**, *115*, 25109–25114; b) R. A. Wahyuono, G. Jia, J. Plentz, A. Dellith, J. Dellith, F. Herrmann-Westendorf, M. Seyring, M. Presselt, G. Andrä, M. Rettenmayr, B. Dietzek, *ChemPhysChem* **2019**, *20*, 3336–3345; c) R. A. Wahyuono, A. Dellith, C. Schmidt, J. Dellith, A. Ignaszak, M. Seyring, M. Rettenmayr, J. Fize, V. Artero, M. Chavarot-Kerlidou, B. Dietzek, *RSC Adv.* **2019**, *9*, 39422–39433.
[39] J. E. Dickeson, L. A. Summers, *Aust. J. Chem.* **1970**, *23*(5), 1023–1027.
[40] V. Nair, A. Augustine, T. G. George, L. G. Nair, *Tetrahedron Lett.* **2001**, *42*, 6763–6765.
[41] G. A. Russell, P. Ngoviwatchai, *J. Org. Chem.* **1989**, *54*, 1836–1842.
[42] M. Wächtler, S. Kupfer, J. Guthmuller, S. Rau, L. Gonzalez, B. Dietzek, *J. Phys. Chem. C* **2012**, *116*, 25664–25676.
[43] a) B. Dietzek, T. Pascher, V. Sundström, A. Yartsev, *Laser Phys. Lett.* **2007**, *4*, 38; b) S. A. Kovalenko, A. L. Dobryakov, J. Ruthmann, N. P. Ernsting, *Phys. Rev. A* **1999**, *59*, 2369–2384.

Manuscript received: February 28, 2020
Revised manuscript received: March 27, 2020
Accepted manuscript online: March 30, 2020
Version of record online: April 24, 2020